From Artificial Atoms to Nanocrystal Molecules:

Preparation and Properties of More Complex Nanostructures

Charina L. Choi and A. Paul Alivisatos

Department of Chemistry, and Material Sciences Division, Lawrence Berkeley National Laboratory, University of California, Berkeley, California 94720; email: APAlivisatos@lbl.gov

Key Words quantum dot, nanocrystal molecule, plasmon ruler, tetrapod, chemical transformations of nanocrystals

Abstract Quantum dots, which have found widespread use in fields such as biomedicine, photovoltaics, and electronics, are often called artificial atoms due to their size-dependent physical properties. Here this analogy is extended to consider artificial nanocrystal molecules, formed from well-defined groupings of plasmonically or electronically coupled single nanocrystals. Just as a hydrogen molecule has properties distinct from two uncoupled hydrogen atoms, a key feature of nanocrystal molecules is that they exhibit properties altered from those of the component nanoparticles due to coupling. The nature of the coupling between nanocrystal atoms and its response to vibrations and deformations of the nanocrystal molecule bonds are of particular interest. We discuss synthetic approaches, predicted and observed physical properties, and prospects and challenges toward this new class of materials.

1. INTRODUCTION

Since their development more than 20 years ago, spherical semiconductor nanocrystals---known as quantum dots---have demonstrated remarkable size-dependent physical properties. Among the phenomena studied are the band gap, radiative rate, melting temperature, and solid-solid phase-transition pressure, which can all be controlled solely by varying the size of the nanocrystal from 100 to up to 10,000 atoms (1--5). Because a quantum dot exhibits discrete and tunable structure in its optical and electrical characteristics, it is often referred to as an artificial atom (**Figure 1**).

Nanocrystal: a crystalline particle with dimensions on the order of nanometers, comprising ~100--10,000 atoms and exhibiting size-dependent physical properties

The ability to make such artificial atoms has developed significantly in the intervening years, and it becomes natural to consider whether artificial molecules may be created from well-defined groupings of single nanocrystals. Just as a hydrogen molecule has markedly different properties from individual hydrogen atoms, a key feature of an artificial molecule is that it should possess significantly altered properties from those of the component nanoparticles. This distinguishes the work described here from many current and important efforts in which, for instance, quantum dots are combined with magnetic nanoparticles to provide for multimodal capabilities (6). The distinct groups of nanoparticles considered here must have strong coupling between the particles.

In this review we examine major efforts by the field to construct and characterize the properties of nanocrystal molecules. We consider nanocrystal molecules in which the individual nanocrystals are coupled via two main mechanisms: plasmon coupling between metal nanocrystals and direct electronic coupling arising from inorganically connected nanocrystals. In both cases we are interested in the nature of the interparticle coupling, and also in how this coupling changes as the nanocrystal molecule vibrates or deforms. Bond vibrations in organic or small molecules can be spectroscopically observed; we see that this is true for alterations or deformations of nanocrystal molecule bonds as well.

2. PLASMONICALLY COUPLED NANOCRYSTAL MOLECULES

A plasmon is a collective oscillation of the valence electrons in a metallic particle. The resonance frequency of a metal plasmon depends critically on the material composition, especially the electron density in the metal. Most metals exhibit plasmon resonances in the far ultraviolet, but in the noble metals Cu, Ag, and Au, there is a d→s interband transition that mixes with the plasmon resonance and shifts it to the visible region of the electromagnetic spectrum. In nanoparticles, the plasmons couple strongly to optical fields, producing intense light-scattering spectra; this effect can be classically described using Mie theory (7). The light scattering from the noble-metal nanoparticles depends strongly on size with intensity varying as the sixth power of the radius. The light-scattering spectrum from a

single noble-metal nanoparticle of 20 nm or larger can readily be observed in a dark-field microscope equipped with a standard tungsten lamp. As two metal nanoparticles are brought into proximity, the charge oscillations couple to each other, resulting in altered optical and electronic behavior that is highly distance-dependent. This coupling effect is exploited in making metal nanocrystal molecules with new capabilities. Plasmon coupling occurs through a dielectric medium and readily extends over distances comparable to the nanocrystal diameter, making it particularly useful for situations in which metal nanoparticles are linked via biological macromolecules.

2.1. Directed Assembly of Metal Nanocrystals Using Biological Macromolecules

There are two reasons for using biological macromolecules to effect the metal nanocrystal assembly. First, biological macromolecules are capable of chemical recognition and assembly to a degree of sophistication that substantially exceeds what is otherwise possible. Thus a wide range of nanocrystal molecules, with a variety of symmetries and degrees of interconnection, can be readily achieved using oligonucleotides or peptides to arrange the nanoparticle assembly. Second, by using biological macromolecules as the glue that holds the nanoparticles together, biological sensing is automatically built into the resulting nanocrystal molecules. Any conformational change in biomolecule linker directly results in a change in the distance between the nanoparticles, which should produce a detectable signal if the nanoparticles are coupled to each other strongly.

Alivisatos and Schultz demonstrated one of the first uses of DNA to organize nanocrystal molecules in 1996, with a sequel experiment following in 1999 (8, 9) (**Figure 2**). In this experiment, Au nanoparticles conjugated to complementary strands of DNA were brought together via Watson-Crick base pairing, resulting in distinct Au nanoparticle dimers and trimers. This work appeared simultaneously with work by Mirkin and Letsinger, who used DNA to assemble Au nanoparticle arrays (10). Indeed, if the nanocrystal is thought of as an artificial atom, then the construction of artificial solids is an important and complementary activity to the construction of artificial molecules (11--13).

The use of biological macromolecules to assemble metal nanocrystals has been further developed to design more complex structures. Nanocrystal assemblies consisting of a central nanocrystal with many satellite nanocrystals attached have been achieved by a variety of methods (14, 15). Chains of metal nanoparticles linked by single-stranded DNA

have been synthesized through the use of DNA ligase and subsequent pair bonding of complementary DNA strands yields chains of metal nanoparticle pairs(16) (**Figure 3*a***). Chiral Au nanoparticle assemblies, adapted from Seeman's (17) complex DNA nanostructures, have been demonstrated in the form of left- and right-handed four-nanoparticle pyramids (18) (**Figure 3*b***). Programmable dynamic behavior of Au nanoparticle assemblies has also been achieved (19) (**Figure 3*c***). Future combinations utilizing these demonstrated operations of central branch points, linear extensions, chirality, and dynamic capabilities can be used to create a wide variety of nanocrystal molecules with tunable collective properties.

2.2. Alternative Methods for Construction of Plasmonic Nanocrystal Molecules

Plasmon-coupled nanocrystal molecules may also be constructed without the aid of biomolecules. For example, spherical metal nanoparticles can assemble together via the polymerization of organic surface ligands. When two thiol ligands of different lengths arrange on the surface of an Au nanoparticle, they form alternating latitude ring-like domains. This phenomenon is not observed on flat surfaces and thus is likely driven by surface curvature. Topological considerations and molecular-dynamics simulations demonstrate that this surface arrangement is possible only if a single thiol molecule sticks out at each pole (20). Stellacci and coworkers (21) demonstrated that the thiol molecules at either end of the particle can be replaced with longer-chain carboxy-terminated molecules, resulting in reactive sites at the particle poles. Diamines are then utilized to polymerize the divalent Au nanoparticle monomers, resulting in Au nanoparticle chains. Alternatively, Novak & Feldheim (22) used stiff thiol-functionalized phenylacetylenes to assemble Ag and Au dimers, trimers, and tetramers.

In addition to particle assembly, varying the nanocrystal shape is an alternative and powerful method for tuning plasmon resonances. This is accomplished mainly by altering synthetic conditions, without the aid of any nanoparticle linker molecules. For example, Au nanorods are grown via a seed-mediated synthesis, with the aspect ratio controlled by varying the amount of cationic surfactant present (23). Au and Ag nanoprisms are synthesized by photochemical or thermal methods (24). In comparison with simple spheres, nanorods and nanoprisms have optical properties much more enhanced and tunable by

variation of the particle dimensions (24a). Au nanoshells are grown by the reduction of Au on the surface of a solid core that is either dissolved, in the case of an Ag core, or plasmon inactive, such as a silica core (25); the optical properties of an Au nanoshell exhibit greater sensitivity to particle dimensions in comparison with its solid counterpart. The use of dielectric cores as a structural synthetic tool has also led to the formation of nanoeggs, nanomatryushkas, and nanorice (**Figure 3*d***), all with unique optical properties (26). The diverse plasmon resonance spectra of these shaped nanoparticles can be thought of as arising from the coupling together of simpler systems, so that these complex shapes, too, are nanocrystal molecules (26, 26a).

2.3. Theoretical Considerations of Plasmonic Nanocrystal Molecules

The ability to design and synthesize plasmon-coupled nanocrystal molecules is significant as new behaviors are predicted for these assemblies. The electromagnetic field--induced charge displacements within two noble-metal particles will couple to each other as the particles are brought together. In analogy with molecular bonding, when two metal nanoparticles are brought close together, the plasmon resonance splits into a lower and a higher frequency mode. Constructive interference will occur between the enhanced fields of each particle, leading to the red-shifting of the lowest-energy coupled plasmon resonance, and an enhanced electromagnetic field in the particle junction (**Figure 4*a***) (27). Similarly, destructive interference produces a mode of higher frequency.

In consistence with the notion of individual nanocrystals as artificial atoms, Nordlander and Halas (26) have contributed greatly to the field by using a method analogous to molecular orbital theory to model the interaction between two plasmonic particles (**Figure 4*b***). The charge oscillations in two metal nanocrystals, with a separation less than their diameter, will strongly couple to each other. The single plasmon resonance of one particle will now split into two resonances: a longitudinal mode, in which the charge oscillations are aligned along the interparticle axis, and a transverse mode, in which the charge oscillations are perpendicular to the interparticle axis. As the two particles get closer together, the longitudinal mode shifts to lower energy, whereas as they move further apart, it shifts to higher energy. In addition, the light-scattering intensity from the longitudinal mode of a pair of strongly coupled particles can be up to four times more intense than that of a single particle. Thus, the plasmon resonance energy and the light-scattering intensity from

plasmon-coupled nanoparticles serve as reporters of interparticle separation and orientation (28). This technique has also been utilized to consider plasmon coupling in trimers and quadramers of metal nanoparticles (29), as well as hollow metal nanospheres (30, 31).

The plasmon shift as a function of interparticle distance also depends greatly on the size, shape, and composition of the metal nanoparticle; the dielectric constant of the surrounding medium; and the direction of light polarization relative to the interparticle axis (31a, 32). Larger nanoparticles exhibit greater plasmon shifts for a given center-to-center distance. Ag nanoparticles generally have sharper plasmon resonances than Au due to a larger polarizability, making the effects of interparticle coupling easier to see (32, 32a). The surface plasmon light-scattering peak of a single particle will red-shift as the dielectric constant of the surrounding medium is increased because the charge oscillations in the metal particle induce a polarization in the dielectric medium. Generally, the effect of local dielectric changes is smaller than effects that arise when another noble-metal nanoparticle is placed nearby, as the second nanoparticle is far more polarizable than the typical dielectric medium.

Care must be taken in calculating the magnitude of the interparticle coupling. It is not enough to include simple dipole-dipole terms to describe the polarizations in each nanoparticle, because the nanoparticles are within a diameter of each other and higher-order terms in a multipole expansion are needed. Pinchuk & Schatz (7) developed a quantitative theory to describe these phenomena. El-Sayed and coworkers (32) provided a scaling description that empirically describes the fractional plasmon shift for an Au nanodisc pair in solution:

$$\frac{\lambda}{\lambda_0} \approx a \bullet \exp\left(\frac{-(R/D)}{\tau}\right), \quad (1)$$

where λ is the plasmon resonance of the Au particle pair, λ_0 is the plasmon resonance of the individual particles, R is the interparticle center-to-center distance, D is the particle diameter, τ is the decay constant, and a is the amplitude of the fractional shift in the system. From the simulation, the authors find that τ has a value of ~0.2; that is, the plasmon coupling decay length is roughly 0.2 times the particle diameter. This value is universal, regardless of particle size (**Figure 4*c***), shape, metal type, and medium dielectric constant,

all of which affect only the amplitude of the fractional shift. Although the expression is calculated for light polarization oriented parallel to the interparticle axis, experimental polarization effects only become significant for larger particles (~87 nm) (33).

2.4. Observed Properties of Plasmonic Molecules and Their Use in Microscopy and Spectroscopy

One feature of plasmon scattering cannot be overemphasized when considering the use of plasmons as reporters in microscopy and spectroscopy: the light scattering from a single noble-metal nanoparticle does not change with time at all. It is just constant. In a noble-nanocrystal molecule, the light scattering will change only if the distance between the nanoparticles changes (small changes due to the variation of the dielectric constant of the surrounding medium can be detected but are an order of magnitude smaller than those due to particle proximity). Otherwise, the spectra are invariant. This is not true of any other type of single-molecule optical label. Organic dyes show intersystem crossing and bleach, lasting only a few tens of seconds under typical single-molecule conditions. Colloidal quantum dots luminesce much longer, but generally also show blinking, with a wide range of on and off times (34, 35). Plasmon resonances do not suffer from these drawbacks. Indeed, plasmonic nanocrystal molecules provide faithful trajectories for the analysis of the conformational changes of individual biological macromolecules.

A starting point for these studies is shown in **Figure 5*a***. When a second particle binds to a single particle immobilized on a surface, the light-scattering intensity increases, and the plasmon peak red-shifts for both Ag and Au particles, as expected (36). This so-called **plasmon ruler** technique has been used to study the cutting of DNA by the EcoRV restriction enzyme (**Figure 5*b***) (37). In this experiment, Au nanoparticle dimers linked by oligonucleotides containing the EcoRV cutting site are deposited on a substrate and imaged in a dark-field microscope. When the enzyme is flowed into the chamber, the plasmon resonance blue-shifts as expected---the second particle flows away as soon as it is cut. The EcoRV enzyme is known to first bend and then cut the DNA, and this can be seen in the light-scattering intensity, which increases slightly and then abruptly decreases as the DNA is cut. The plasmon ruler has been calibrated to correlate the distance between Au nanoparticle pairs with spectral shifts and has proved useful for further biological studies, including the observation of single caspase-3 enzyme cutting events in vivo (38).

Plasmon ruler: a tool utilizing the light-scattering spectra of a plasmonic nanocrystal molecule to observe distance-dependent phenomena

Fluorescence resonance energy transfer techniques have been extremely useful in studying conformational changes in many systems (39, 40). However, their use is limited by the lifetime and distance dependency (~$1/R^6$) of the dyes: Typically tens of seconds and distances of 1--10 nm are accessible in a given experiment. Because of the invariant plasmon signal over time, and the size-dependent near-exponential distance decay ($e^{-R/D}$, Equation 1), plasmon rulers provide an additional tool capable of studying distances from 1 to 70 nm, for any length of time desired.

The electromagnetic field enhancement at the junction between two or more metal particles has been observed experimentally (41--43). This has proved useful for surface-enhanced Raman spectroscopy studies down to the single-molecule level. Indeed, many unique metal nanostructures have been designed for this purpose (44, 45). As we focus here on plasmon spectral shift effects, we refer the reader to comprehensive reviews on surface-enhanced Raman spectroscopy (46, 47) and note that there have been important applications of metal nanocrystal molecules in this area. The enhanced electromagnetic field effect has also been utilized for electromagnetic energy transport and subwavelength optical waveguiding (48, 49).

3. ELECTRONICALLY COUPLED NANOCRYSTAL MOLECULES

Plasmon coupling occurs through space or a dielectric medium. Another way to produce coupling between two **nanocrystals** is through tunneling and exchange coupling of electrons. This is precisely analogous to molecular bonding. For this to be a significant effect, two nanocrystals need to be joined by a medium through which the quantum confined electrons can tunnel. The effective masses of the electrons in a semiconductor quantum dot can vary from 1 to 0.01. The length scale over which two dots can then be coupled will depend critically on the potential of the electron in the medium that separates the two dots. Generally, it is necessary to try to lower the potential as much as possible to promote the coupling; for this reason, it is common to attempt to grow dots that are interconnected by an inorganic semiconductor medium, in which the electron potential is

higher than that in the dots themselves, but lower than in vacuum or typical dielectric or insulating media. Thus, for such nanocrystal molecules to be studied, it becomes important to be able to grow complex nanocrystals in which regions of differing composition are connected together in well-defined ways. Although there are many versions of electronically coupled nanocrystal molecules, we highlight one case, that of semiconductor **tetrapods**, because of their beautiful symmetry (they are analogous to a methane molecule) and because the influence of mechanical deformations on their electronic properties can be investigated.

Tetrapod: an electronically coupled semiconductor nanocrystal molecule, with four arms branched from a central core at the tetrahedral angle

3.1. Synthesis of Nanocrystal Molecules with Inorganic Interconnections

Semiconductor nanocrystals, typically consisting of II-VI or III-V semiconductor materials, have been synthesized via gas-phase, molecular-beam epitaxy, and colloidal methods. We focus here on colloidal synthesis, in which the resulting nanocrystal can be considered a chemical reagent, able to be dissolved in a fluid, spun into a polymer, attached to an electrical circuit, or reacted with other chemicals (2, 50). The colloidal synthesis of semiconductor nanocrystals has developed significantly from quantum dots to nanocrystal molecules of many different shapes, sizes, and chemical compositions (**Figure 6**) (51--53). Dots (**Figure 6*a***), rods (**Figure 6*b***), discs, and tetrapods (**Figure 6*c***) allow for nanocrystal molecules extended in zero-, one-, two-, and three-dimensions, respectively.

Shape control to achieve nanocrystal molecules is largely accomplished by controlling reaction temperature, which favors one crystal structure over another, and the organic surfactant molecules used, which bind to selective crystal faces and promote growth of other less-protected facets. For example, a tetrapod consists of a zinc-blende (cubic) core with four {111} facets at the tetrahedral angle, each projecting a wurtzite rod terminated with the (0001) facet (54). The temperature is controlled during the synthesis to favor nanocrystal nucleation in the zinc-blende structure, and subsequent wurtzite growth. Alkylphosphonate ligands such as methyl- and hexyl-phosophonic acid (55--57) and quaternary ammonium salt compounds (58) preferentially bind to specific crystal facets to facilitate tetrapod synthesis.

Core/shell particles, comprising a shell grown epitaxially on a core particle of different material, add another layer of complexity and control to the nanocrystal molecule family. Typically, the core is synthesized first by traditional colloidal methods, and the shell is grown either by successive monolayer adsorption or quick nucleation followed by growth on the nanocrystal core. Type I band alignment core/shell heterostructures with the larger band-gap material as the shell result in extremely bright nanocrystals, as both electron and hole carriers are confined to the core. These nanoheterostructures were first demonstrated by Bawendi and coworkers (59), who synthesized CdSe/ZnS quantum dots with 30%--50% quantum yields at room temperature. Such structures are now routinely used, particularly in biological fluorescence-tagging experiments. Type II core/shell heterostructures allow the electron and hole to be segregated to different materials, which is ideal for many photovoltaic and catalytic designs. Other arrangements of wave-function confinement and delocalization are possible via careful choice of core and shell material.

Hollow particles and nested or yolk-shell nanocrystal molecules are synthesized by leveraging the Kirkendall effect: that ions diffuse through interfaces at different rates (60). The deliberate selection of core and shell materials followed by successive oxidation or sulfidization results in partially hollow, nested particles, leading to fully hollow spheres upon longer reaction times. These nanocrystals are used in surface and catalysis studies (61).

Of particular note are the Au-tipped semiconductor nanocrystal molecules demonstrated by Banin and coworkers (62, 63), the first observed metal-semiconductor contact within a colloidal nanocrystal. Metal regions on semiconductor nanocrystals are an interesting class of more complex nanocrystal molecules that provide additional handles for electrical contacts (63a) or biological functionalization via thiol or amine linkers. Current methods provide nonepitaxial Au deposition on semiconductor structures; the Au tip size may be increased by further reduction of the metal in solution. Au-tipped tetrapods bear a striking resemblance to the Au-tipped pyramids constructed by DNA assembly mentioned above (18). These two structures provide a direct comparison between plasmonic through-space and electronic coupling of four tetrahedrally related Au particles.

3.2. Theoretical Considerations of Electronically Coupled Nanocrystal Molecules

Wang and coworkers have developed the semiempirical pseudopotential and ab initio methods to model electron and hole wave-functions in semiconductor nanocrystals. We direct the reader to other literature on this subject (64--66), noting that the optical and electronic properties of a nanocrystal are clearly dependent on nanocrystal shape from these calculations (**Figure 7*a--c***) (67). These theoretical studies are consistent with the concept of rods and tetrapods (and other shapes) as nanocrystal molecules with properties distinct from a series of uncoupled dots in the same geometric arrangement. Furthermore, the mechanical properties of a nanocrystal, related to its shape, are inherently linked to its optoelectronic properties. Schrier et al. (68) predicted that when the top arm of a tetrapod is mechanically compressed while its three supporting arms are flattened along the substrate, inducing arm bending, the electron and hole wave functions of a tetrapod are spatially altered; strain in the top arm reduces the probability of electron or hole localization in that arm (**Figure 7*c,d***). The resulting wave-function overlap results in a red shift of the energy gap. This calculation was recently experimentally confirmed (69) and is discussed further in Section 3.3.

3.3. Observed Properties of Semiconductor Nanocrystal Molecules

Semiconductor nanocrystal molecules exhibit altered optical, electronic, and mechanical properties from their quantum-dot counterparts (**Figure 8**). As the aspect ratio of a wurtzite dot is increased along the c-axis to form a rod, the optoelectronic structure changes due to the inherent dipole in the rod structure (the two faces perpendicular to the c-axis are not equivalent). The particle begins to emit polarized light (69a, 65) as well as exhibit electric field-dependent photoluminescence (69b). In the case of CdSe/CdS core/shell rods (57, 70, 71), in which the hole is localized in the CdSe core whereas the electron is more delocalized over the core and the CdS shell (72--74), the changes in optoelectronic properties are more pronounced (**Figure 8*a***). As the length of the CdS rod shell is increased, the electron and hole wave-function overlap is decreased, leading to a decrease in the radiative decay rate. An external electric field applied to the CdSe/CdS rod additionally affects carrier wave-function localization and thus optoelectronic properties (75).

Even more so than rods, coupled behavior is observed in the optoelectronic properties of tetrapods. In a single-electron transistor experiment, rod and tetrapod particles are immobilized on a 10-nm Si_3N_4 dielectric substrate with a metal back gate, and are contacted

by electron beam lithography with Pd electrodes at both ends of the rod, or three arms of a tetrapod (with the fourth arm protruding upward). The electrical current as a function of voltage is measured for many gate voltages, and the differential conductance ($\partial I/\partial V$) is plotted as a function of V and V_g (**Figure 8*b***). In the case of a single rod transistor, we observe a smooth set of Coulomb diamonds, indicating a single Coulomb-charging energy ladder (**Figure 8*b*, panel i**). This is similar to that observed for a single dot. In the case of a single tetrapod transistor, two types of behavior are observed. The first is a sawtooth-like Coulomb diamond structure (**Figure 8b, panel ii**), a signature akin to single-electron hopping in a system of weakly coupled quantum dots (76). This behavior results from the electron being transported through the arm-branch point- arm in series: modeled, to the simplest approximation, as three Coulomb-charging energy ladders. The second tetrapod transistor behavior exhibits a large Coulomb diamond with two or three smaller diamonds alternating along the V_g axis (**Figure 8*b*, panel iii**). This behavior is expected for a strongly coupled arm-branch point-arm system, with the charge carrier delocalized throughout the tetrapod, similar to lithographically patterned dots on a two-dimensional electron gas. Thus we see that a single tetrapod nanostructure behaves electronically as a collection of coupled quantum dots (77).

The optoelectronic coupling of tetrapods is sensitive to mechanical deformation (**Figure 8*c***). That unique mechanical properties are observed for tetrapods as compared with dots and rods seems intuitive, as particle shape is clearly tied to its response to stress and strain. Nie and colleagues (78) have observed strain-dependent optical properties of core/shell quantum dots with synthetically inherent internal stress. In these materials, a shell is epitaxially grown onto a core of softer material. As the shell thickness is increased, the softer core experiences increased strain, leading to an optical band-gap red shift. Ensemble measurements of CdSe/CdS core/shell dots, rods, and tetrapods all demonstrate a photoluminescence peak blue-shift with increasing pressure under hydrostatic pressure conditions (near-isotropic compression) in a diamond anvil cell (DAC) (69). This results from increased atomic orbital overlap within the crystal, and is consistent with previous measurements on bulk and nanocrystal CdSe (4). However, upon application of pressure when solubilized in a nonhydrostatic medium (anisotropic compression), an additional photoluminescence peak at lower energy is observed for all three particle morphologies.

This peak is attributed to a fraction of the particles within the DAC experiencing nonhydrostatic conditions. The difference between the two peaks reveals the net effect of deviatoric stress on the particles. Tetrapod nanocrystals are most greatly affected by net deviatoric stresses, with greater than 95% of the population affected by nonhydrostaticity; these particles exhibit a photoluminescence red shift with increasing anisotropic deformation. Because the strain state inside a DAC cannot be determined, future experiments are required to calibrate the fluorescence shift with force. With further development, these tetrapods may be effective as optical sensors of externally applied stress (69).

DAC: diamond anvil cell

3.4. Chemical Transformations in Semiconductor Nanocrystals

Just as organic molecules may undergo chemical reactions, inorganic nanocrystal molecules may also undergo chemical transformations. Branching of nanocrystals, analogous to organic dendrimer formation, leads to tetrapod and multipod particles. Addition reactions in nanocrystals result in core/shell, nested, or hollow structures. Simple substitution reactions in particular highlight the ability of nanocrystals to transform as molecular entities. These reactions are demonstrated via a cation exchange mechanism. For example, CdSe quantum dots will quickly transform to Ag_2Se dots upon addition of excess Ag^+ in solution (79). The reaction is fully reversible, and CdSe dots are recovered upon addition of excess Cd^{2+} (**Figure 9*a***). Partial cation exchange has also been demonstrated, with the resultant nanocrystal morphology highly dependent on choice and concentration of cation (80, 81). For example, when CdS nanorods are partially exchanged with Cu^{2+}, a binary nanorod structure forms with Cu_2S at one or both ends of the nanorod (**Figure 9*b***). When CdS nanorods are partially exchanged with Ag^+, however, the CdS rod becomes partially striped with Ag_2S at regularly spaced intervals along the rod (**Figure 6*e***). The interfacial strain between the two lattice structures and the chemical interaction dictates the resultant partially exchanged morphology. Full cation exchange of the CdS nanorod results in fully Cu_2S or Ag_2S nanorods.

That shape is highly preserved while the nanocrystal composition is thoroughly transformed into a different semiconductor material is remarkable. This observation suggests that cation exchange may be a new route toward the synthesis of nanocrystal

molecules with complex compositions. Indeed, recent work has shown that semiconductor nanocrystals difficult to synthesize by established colloidal methods, e.g. PbS nanocrystals, can be achieved through a cation exchange mechanism (82).

Exchange, addition, and branching reactions result in a core set of transformation operations that can be performed sequentially in any order. The discovery of additional transformational tools and further development of multistep nanocrystal syntheses will result in a wide library of inorganic nanocrystals with a variety of properties.

4. IN SITU ELECTRON MICROSCOPY FOR OBSERVATION OF NANOCRYSTAL MOLECULE FORMATION AND DYNAMICS

As discussed above, many types of nanocrystal molecules can be synthesized and that unique properties distinct from those of the individual nanocrystal building blocks are obtained. The size, shape, structure, and composition of these particles can be characterized using transmission electron microscopy. While the formation of such structures may be monitored roughly during formation by characterization of aliquots from synthesis, an ideal tool would enable visualization and characterization of nanocrystal molecule formation in situ. One such technique has recently been developed and used to observe the formation of Pt nanocrystals in real time (83). In this study, Pt nanoparticle precursors are injected into a liquid cell holder and placed into the transmission electron microscope, with growth of Pt nanocrystals catalyzed by the electron beam. Nanocrystals are observed to form both via monomer addition and particle coalescence (**Figure 10**). This observation is a first step toward understanding simple nanocrystal formation mechanisms and kinetics. Future work will investigate the formation of more complex nanocrystals via reactions such as branching or cation exchange, as well as nanocrystal transformations during catalysis. These experiments are underway.

5. FUTURE OUTLOOK

Nanoscience has opened up the ability to create whole new classes of materials with designed properties. Early work in size control and characterization established that the artificial atom concept could be successfully applied to colloidal nanoparticles of inorganic solids, as if the periodic table itself acquired a third dimension corresponding to size. In the

past decade, this analogy has developed further, with clear demonstrations that artificial atoms can be coupled together to create artificial nanocrystal molecules. Many of these effects have only been demonstrated at a proof-of-principle level, with limited numbers and types of nanoparticles connected to each other. As we learn to control the spatial arrangements of nanoparticles in new and more advanced ways, it should be possible to create ever more intricate and controlled nanocrystal molecules.

SUMMARY POINTS

1. Well-defined groupings of single nanocrystals may couple to form a nanocrystal molecule. The physical properties of a nanocrystal molecule, including its optical, electronic, and mechanical properties, are significantly altered from those of the component nanoparticles due to the interparticle coupling.
2. Plasmonically coupled nanocrystal molecules are distinct groupings of coupled metal nanocrystals that may be assembled together via biological macromolecules, organic linkers, or synthesis-mediated shape control.
3. Electronically coupled nanocrystal molecules are distinct groupings of nanocrystals coupled through tunneling and exchange coupling of electrons, typically through an inorganic semiconductor medium.
4. Similar to organic molecules, inorganic nanocrystals may undergo chemical transformations, including exchange, addition, and branching reactions.
5. In situ transmission electron microscopy has been recently developed to observe Pt nanocrystal formation in real time. Further advancement of the technique may provide the capability to visualize the formation of more complex nanocrystal molecules.
6. Nanoscience has opened up the ability to create new classes of materials with designed properties. Future progress should allow the creation of ever more intricate and controlled nanocrystal molecules.

DISCLOSURE STATEMENT

The authors are not aware of any affiliations, memberships, funding, or financial holdings that might be perceived as affecting the objectivity of this review.

ACKNOWLEDGEMENTS

The authors thank Jonathan Chou, Jessy L. Baker, Young-wook Jun, and Prashant K. Jain for helpful discussions and critical reading of the manuscript. C.L.C. was supported by the NIH Roadmap Initiative in Nanomedicine through a Nanomedicine Development Centre award (PN2EY016546) and A.P.A. was supported by the Director, Office of Science, Office of Basic Energy Sciences, of the United States Department of Energy under Contract DE-AC02-05CH11231.

LITERATURE CITED

1. Goldstein AN, Echer CM, Alivisatos AP. 1992. Melting in semiconductor nanocrystals. *Science* 256:1425--27
2. Alivisatos AP. 1996. Perspectives on the physical chemistry of semiconductor nanocrystals. *J. Phys. Chem.* 100:13226--39
3. Vossmeyer T, Katsikas L, Giersig M, Popovic IG, Diesner K, et al. 1994. CdS nanoclusters: synthesis, characterization, size dependent oscillator strength, temperature shift of the excitonic transition energy, and reversible absorbance shift. *J. Phys. Chem.* 98:7665--73

4. Tolbert SH, Alivisatos AP. 1995. High-pressure structural transformations in semiconductor nanocrystals. *Annu. Rev. Phys. Chem.* 46:595--626

5. Alivisatos AP. 1996. Semiconductor clusters, nanocrystals, and quantum dots. *Science* 271:933--37

6. Jun Y, Choi J, Cheon J. 2007. Heterostructured magnetic nanoparticles: their versatility and high performance capabilities. *Chem. Commun.* 12:1203--14

7. Pinchuk A, Schatz G. 2005. Anisotropic polarizability tensor of a dimer of nanospheres in the vicinity of a plane substrate. *Nanotechnology* 16:2209--17

8. Alivisatos AP, Johnsson KP, Peng X, Wilson TE, Loweth CJ, et al. 1996. Organization of 'nanocrystal molecules' using DNA. *Nature* 382:609--11

9. Loweth CJ, Caldwell WB, Peng X, Alivisatos AP, Schultz PG. 1999. DNA-based assembly of gold nanocrystals. *Angew. Chem. Int. Ed. Engl.* 38:1808--12

10. Mirkin CA, Letsinger RL, Mucic RC, Storhoff JJ. 1996. A DNA-based method for rationally assembling nanoparticles into macroscopic materials. *Nature* 382:607--9

11. Murray CB, Kagan CR, Bawendi MG. 2000. Synthesis and characterization of monodisperse nanocrystals and close-packed nanocrystal assemblies. *Annu. Rev. Mater. Sci.* 30:545--610

12. Rogach AL, Talapin DV, Shevchenko EV, Kornowski A, Haase M, Weller H. 2002. Organization of matter on different size scales: monodisperse nanocrystals and their superstructures. *Adv. Funct. Mater.* 12:653--64

13. Kovalenko MV, Scheele M, Talapin DV. 2009. Colloidal nanocrystals with molecular metal chalcogenide surface ligands. *Science* 324:1417--20

14. Fu A, Micheel CM, Cha J, Chang H, Yang H, Alivisatos AP. 2004. Discrete nanostructures of quantum dots/Au with DNA. *J. Am. Chem. Soc.* 126:10832--33

15. Maye MM, Nykypanchuk D, Cuisinier M, Van Der Lelie D, Gang O. 2009. Stepwise surface encoding for high-throughput assembly of nanoclusters. *Nat. Mater.* 8:388--91

16. Claridge SA, Mastroianni AJ, Au YB, Liang HW, Micheel CM, et al. 2008. Enzymatic ligation creates discrete multinanoparticle building blocks for self-assembly. *J. Am. Chem. Soc.* 130:9598--605

17. Seeman NC. 1999. DNA engineering and its application to nanotechnology. *Trends Biotechnol.* 17:437--43

18. Mastroianni AJ, Claridge SA, Alivisatos AP. 2009. Pyramidal and chiral groupings of gold nanocrystals assembled using DNA scaffolds. *J. Am. Chem. Soc.* 131:8455--59

19. Aldaye FA, Sleiman HF. 2007. Dynamic DNA templates for discrete gold nanoparticle assemblies: control of geometry, modularity, write/erase and structural switching. *J. Am. Chem. Soc.* 129:4130--31

20. Perepichka DF, Rosei F. 2007. Metal nanoparticles: from "artificial atoms" to "artificial molecules". *Angew. Chem. Int. Ed. Engl.* 46: 6006--8

21. DeVries GA, Brunnbauer M, Hu Y, Jackson AM, Long B, et al. 2007. Divalent metal nanoparticles. *Science* 315:358--61

22. Novak JP, Feldheim DL. 2000. Assembly of phenylacetylene-bridged silver and gold nanoparticle arrays. *J. Am. Chem. Soc.* 122:3979--80

23. Johnson CJ, Dujardin E, Davis SA, Murphy CJ, Mann S. 2002. Growth and form of gold nanorods prepared by seed-mediated, surfactant-directed synthesis. *J. Mater. Chem.* 12:1765--70

24. Millstone JE, Hurst SJ, Métraux GS, Cutler JI, Mirkin CA. 2009. Colloidal gold and silver triangular nanoprisms. *Small* 5:646—64

24a. Kelly KL, Coronado E, Zhao LL, Schatz GC. 2003. The optical properties of metal nanoparticles: the influence of size, shape, and dielectric environment. *J. Phys. Chem. B.* 107:668-77

25. Oldenburg S, Averitt RD, Westcott S, Halas NJ. 1998. Nanoengineering of optical resonances. *Chem. Phys. Lett.* 288:243--47

26. Wang H, Brandl DW, Nordlander P, Halas NJ. 2007. Plasmonic nanostructures: artificial molecules. *Acc. Chem. Res.* 40:53—62

26a. Jain PK, Eustis S, El-Sayed MA. 2006. Plasmon coupling in nanorod assemblies: optical absorption, discrete dipole approximation simulation, and exciton-coupling model. *J. Phys. Chem. B.* 110:18243-53

27. Talley CE, Jackson JB, Oubre C, Grady NK, Hollars CW, et al. 2005. Surface-enhanced Raman scattering from individual Au nanoparticles and nanoparticle dimer substrates. *Nano Lett.* 5:1569--74

28. Nordlander P, Oubre C, Prodan E, Li K, Stockman MI. 2004. Plasmon hybridization in nanoparticle dimers. *Nano Lett.* 4:899--903

29. Brandl DW, Oubre C, Nordlander P. 2005. Plasmon hybridization in nanoshell dimers. *J. Chem. Phys.* 123:024701

30. Prodan E, Radloff C, Halas NJ, Nordlander P. 2003. A hybridization model for the plasmon response of complex nanostructures. *Science* 302:419--22

31. Prodan E, Nordlander P. 2004. Plasmon hybridization in spherical nanoparticles. *J. Chem. Phys.* 120:5444—54

31a. Jain PK, El-Sayed MA. 2008. Plasmon coupling and its universal size scaling in nanostructures of complex geometry: elongated particle pairs and nanosphere trimers. *J. Phys. Chem. C.* 112:4954--60

32. Jain PK, Huang W, El-Sayed MA. 2007. On the universal scaling behavior of the distance decay of plasmon coupling in metal nanoparticle pairs: plasmon ruler equation. *Nano Lett.* 7:2080—88

32a. Gunnarsson L, Rindzevicius T, Prikulis J, Kasemo B, Käll M, Zou S, Schatz GC. 2005. Confined plasmons in nanofabricated single silver particle pairs---experimental observations of strong interparticle interactions. *J. Phys. Chem. B.* 109:1079-87

33. Reinhard BM, Siu M, Agarwal H, Alivisatos AP, Liphardt J. 2005. Calibration of dynamic molecular rulers based on plasmon coupling between gold nanoparticles. *Nano Lett.* 5:2246--52

34. Nirmal M, Dabbousi BO, Bawendi MG, Macklin JJ, Trautman JK, et al. 1996. Fluorescence intermittency in single cadmium selenide nanocrystals. *Nature* 383:802--4

35. Kuno M, Fromm DP, Hamann HF, Gallagher A, Nesbitt DJ. 2000. Nonexponential "blinking" kinetics of single CdSe quantum dots: a universal power law behavior. *J. Chem. Phys.* 112:3117--20

36. Sönnichsen C, Reinhard BM, Liphardt J, Alivisatos AP. 2005. A molecular ruler based on plasmon coupling of single gold and silver nanoparticles. *Nat. Biotechnol.* 23:741--45

37. Reinhard BM, Sheikholeslami S, Mastroianni A, Alivisatos AP, Liphardt J. 2007. Use of plasmon coupling to reveal the dynamics of DNA bending and cleavage by single EcoRV restriction enzymes. *Proc. Natl. Acad. Sci. USA* 104:2667--72

38. Jun Y, Sheikholeslami S, Hostetter D, Tajon C, Craik C, Alivisatos AP. 2009. Single molecule imaging of signaling proteins activated in live cells by the use of plasmon rulers.

Proc. Natl. Acad. Sci. USA. In Press 39. Wu PG, Brand L. 1994. Resonance energy transfer: methods and applications. *Anal. Biochem.* 218:1--13

40. Jares-Erijman EA, Jovin TM. 2003. FRET imaging. *Nat. Biotechnol.* 21:1387--95
41. Michaels AM, Jiang J, Brus L. 2000. Ag nanocrystal junctions as the site for surface-enhanced Raman scattering of single rhodamine 6G molecules. *J. Phys. Chem. B.* 104:11965--71
42. Markel VA, Shalaev VM, Zhang P, Huynh W, Tay L, et al. 1999. Near-field optical spectroscopy of individual surface-plasmon modes in colloid clusters. *Phys. Rev. B* 59:10903--9
43. Bozhevolnyi SI, Markel VA, Coello V, Kim W, Shalaev VM. 1998. Direct observation of localized dipolar excitations on rough nanostructured surfaces. *Phys. Rev. B* 58:11441--48
44. Fromm DP, Sundaramurthy A, Kinkhabwala A, Schuck PJ, Kino GS, Moerner WE. 2006. Exploring the chemical enhancement for surface-enhanced Raman scattering with Au bowtie nanoantennas. *J. Chem. Phys.* 124:061101
45. Bidault S, de Abajo JG, Polman A. 2008. Plasmon-based nanolenses assembled on a well-defined DNA template. *J. Am. Chem. Soc.* 130:2750--51
46. Moskovits M. 1985. Surface-enhanced spectroscopy. *Rev. Mod. Phys.* 57:783--826
47. Stiles PL, Dieringer JA, Shah NC, Van Duyne RP. 2008. Surface-enhanced Raman spectroscopy. *Annu. Rev. Anal. Chem.* 1:601--26
48. Maier SA, Atwater HA. 2005. Plasmonics: localization and guiding of electromagnetic energy in metal/dielectric structures. *J. Appl. Phys.* 98:011101
49. Lai S, Link S, Halas NJ. 2007. Nano-optics from sensing to waveguiding. *Nat. Photonics* 1:641--48
50. Yin Y, Alivisatos AP. 2005. Colloidal nanocrystal synthesis and the organic-inorganic interface. *Nature* 437:664--70
51. Peng X, Manna L, Yang WD, Wickham J, Scher E, et al. 2000. Shape control of CdSe nanocrystals. *Nature* 404:59--61
52. Milliron DJ, Hughes SM, Cui Y, Manna L, Li JB, et al. 2004. Colloidal nanocrystal heterostructures with linear and branched topology. *Nature* 430:190--95
53. Manna L, Scher EC, Alivisatos AP. 2000. Synthesis of soluble and processable rod-, arrow-, teardrop-, and tetrapod-shaped CdSe nanocrystals. *J. Am. Chem. Soc.* 122:12700--6

54. Manna L, Milliron DJ, Meisel A, Scher EC, Alivisatos AP. 2003. Controlled growth of tetrapod-branched inorganic nanocrystals. *Nat. Mater.* 2:382--85

55. Carbone L, Kudera S, Carlino E, Parak WJ, Giannini C, et al. 2005. Multiple wurtzite twinning in CdTe nanocrystals indicued by methylphosphonic acid. *J. Am. Chem. Soc.* 128:748--55

56. Yu WW, Wang YA, Peng X. 2003. Formation and stability of size-, shape-, and structure-controlled CdTe nanocrystals: ligand effects on monomers and nanocrystals. *Chem. Mater.* 15:4300--8

57. Talapin DV, Nelson JH, Shevchenko EV, Aloni S, Sadtler B, Alivisatos AP. 2007. Seeded growth of highly luminescent CdSe/CdS nanoheterostructures with rod and tetrapod morphologies. *Nano Lett.* 7:2951--59

58. Asokan S, Krueger KM, Colvin VL, Wong MS. 2007. Shape-controlled synthesis of CdSe tetrapods using cationic surfactant ligands. *Small* 3:1164--69

59. Dabbousi BO, Rodriguez-Viejo J, Mikulec FV, Heine JR, Mattoussi H, et al. 1997. (CdSe)ZnS core-shell quantum dots: synthesis and characterization of a size series of highly luminescent nanocrystallites. *J. Phys. Chem. B* 101:9463--75

60. Yin YD, Rioux RM, Erdonmez CK, Hughes SM, Somorjai GA, Alivisatos AP. 2004. Formation of hollow nanocrystals through the nanoscale Kirkendall effect. *Science* 304:711--14

61. Kim SH, Yin Y, Alivisatos AP, Somorjai GA, Yates JT. 2007. IR spectroscopic observation of molecular transport through Pt@CoO yolk-shell nanostructures. *J. Am. Chem. Soc.* 129:9510--13

62. Mokari T, Rothenberg E, Popov I, Costi R, Banin U. 2004. Selective growth of metal tips onto semiconductor quantum rods and tetrapods. *Science* 304:1787--90

63. Saunders AE, Popov I, Banin U. 2006. Synthesis of hybrid CdS-Au colloidal nanostructures. *J. Phys. Chem. B* 110:25421--29

63a.. Sheldon MT, Trudeau PE, Mokari T, Wang, LW, Alivisatos AP. 2009. Enhanced semiconductor nanocrystal conductance via solution grown contacts. *Nano Lett.* Articles ASAP online

64. Wang LW, Zunger A. 1995. Local-density-derived semiempirical pseudopotentials. *Phys. Rev. B* 51:17398--416

65. Hu J, Li L, Wang LW, Alivisatos AP. 2002. Semiempirical pseudopotential calculation of electronic states of CdSe quantum rods. *J. Phys. Chem.* 106:2447--52

66. Wang LW. 2010. Novel electronic structure algorithms for nanoscience. *Annu. Rev. Phys. Chem.* 61:In press

67. Li J, Wang LW. 2003. Shape effects on electronic states of nanocrystals. *Nano Lett.* 3:1357--63

68. Schrier J, Lee B, Wang LW. 2008. Mechanical and electronic-structure properties of compressed CdSe tetrapod nanocrystals. *J. Nanosci. Nanotechnol.* 8:1994--98

69. Choi CL, Koski KJ, Sivasankar S, Alivisatos AP. 2009. Strain-dependent photoluminescence behavior of CdSe/CdS nanocrystals with spherical, linear, and branched topologies. *Nano Lett.* 9:3544-3549 69a. Hu JT, Li LS, Yang WD, Manna L, Wang LW, et al. 2001. Linearly polarized emission from colloidal semiconductor quantum rods. *Science* 292:2060-2063

69b. Rothenberg E, Kazes M, Shaviv E, Banin U. 2005. Electric field induced switching of the fluorescence of single semiconductor quantum rods. *Nano Lett.* 5:1581-1586

70. Talapin DV, Koeppe R, Götzinger S, Kornowski A, Lupton JM, et al. 2003. Highly emissive colloidal CdSe/CdS heterostructures of mixed dimensionality. *Nano Lett.* 3:1677--81

71. Carbone L, Nobile C, De Giorgi M, Della Sala F, Morello G, et al. 2007. Synthesis and micrometer-scale assembly of colloidal CdSe/CdS nanorods prepared by a seeded growth approach. *Nano Lett.* 7:2942--50

72. Peng X, Schlamp MC, Kadavanich A, Alivisatos AP. 1997. Epitaxial growth of highly luminescent CdSe/CdS core/shell nanocrystals with photostability and electronic accessibility. *J. Am. Chem. Soc.* 119:7019--29

73. Müller J, Lupton JM, Rogach AL, Feldmann J, Talapin DV, Weller H. 2004. Monitoring surface charge movement in single elongated semiconductor nanocrystals. *Phys. Rev. Lett.* 93:167402

74. Steiner D, Dorfs D, Banin U, Della Sala F, Manna L, Millo O. 2008. Determination of band offsets in heterostructured colloidal nanorods using scanning tunneling spectroscopy. *Nano Lett.* 8:2954--58

75. Müller J, Lupton JM, Lagoudakis PG, Schindler F, Koeppe R, et al. 2005. Wave function engineering in elongated semiconductor nanocrystals with heterogeneous carrier confinement. *Nano Lett.* 5:2044--49

76. Van Der Wiel WG, De Franceschi S, Elzerman JM, Fujisawa T, Tarucha S, Kouwenhoven LP. 2003. Electron transport through double quantum dots. *Rev. Mod. Phys.* 75:1--22

77. Cui Y, Banin U, Björk MT, Alivisatos AP. 2005. Electrical transport through a single nanoscale semiconductor branch point. *Nano Lett.* 5:1519--23

78. Smith AM, Mohs AM, Nie S. 2009. Tuning the optical and electronic properties of colloidal nanocrystals by lattice strain. *Nat. Nanotechnol.* 4:56--63

79. Son DH, Hughes SM, Yin Y, Alivisatos AP. 2004. Cation exchange reactions in ionic nanocrystals. *Science* 306:1009--12

80. Robinson RD, Sadtler B, Demchenko DO, Erdonmez CK, Wang LW, Alivisatos AP. 2007. Spontaneous superlattice formation in nanorods through partial cation exchange. *Science* 317:355--58

81. Sadtler B, Demchenko DO, Zheng H, Hughes SM, Merkle MG, et al. 2009. Selective facet reactivity during cation exchange in cadmium sulfide nanorods. *J. Am. Chem. Soc.* 131:5285--93

82. Luther JM, Zheng H, Sadtler B, Alivisatos AP. 2009. Synthesis of PbS nanorods and other ionic nanocrystals of complex morphology by sequential cation exchange reactions. *J. Am. Chem. Soc.* In press

83. Zheng H, Smith RK, Jun Y, Kisielowski C, Dahmen U, Alivisatos AP. 2009. Observation of single colloidal platinum nanocrystal growth trajectories. *Science* 324:1309--12

Figure captions.

Figure 1 A single isolated quantum dot as an artificial atom. (*a*) Density of states in one band of a semiconductor as a function of dimension. The energy levels become discrete near the Fermi level for "0D" crystals. (*b*) Transmission electron micrograph of a colloidally prepared wurtzite (wz)-CdSe nanocrystal with well-defined facets. The surface is passivated with organic surfactants. Figure taken from Reference 5, reprinted with permission from AAAS.

Figure 2 DNA-directed assembly of 5- and 10-nm Au particles into dimer and trimer nanocrystal molecules. Figure adapted from Reference 9.

Figure 3 Plasmonically coupled nanocrystal molecules. (*a*) Tetramers and hexamers of 10-nm Au nanocrystals can be assembled as chains of particle pairs using DNA and enzymatic ligation. Figure adapted with permission from Reference 16. Copyright 2008 American Chemical Society. (*b*) DNA directed assembly of chiral nanostructures with 5-, 10-, 15-, and 20-nm Au nanocrystals at the pyramid vertices. Figure adapted with permission from Reference 18. Copyright 2009 American Chemical Society. Scale bar is 20 nm in panels *a* and *b*. (*c*)

Write/erase function in dynamic DNA templates demonstrated by (*i*) writing three 15-nm Au particles into triangles, (*ii*) removing a specific particle using a complementary eraser strand, and (*iii*) rewriting with a 5-nm particle; scale bar is 50 nm. Figure taken, in part, with permission from Reference 19. Copyright 2007 American Chemical Society. (*d*) Colloidally constructed plasmonic nanocrystal molecules: (*i*) Au nanoshells, (*ii*) Au nanoeggs, (*iii*) Au nanorice, and (*iv*) Au nanomatryushkas; scale bar is 100 nm. Figure adapted with permission from Reference 26. Copyright 2007 American Chemical Society.

Figure 4 New behaviors are predicted for plasmonically coupled nanocrystal molecules. (*a*) Electromagnetic near-field enhancement at the excitation laser wavelength (633 nm) for an adjacent Au nanosphere pair with the interparticle axis parallel to the incident polarization, calculated using the finite-difference time-domain method. The color scale represents the electromagnetic field enhancement ($|E|$). Figure adapted with permission from Reference 27. Copyright 2005 American Chemical Society. (*b*) Schematic of plasmon hybridization in a metal nanocrystal dimer. The individual nanosphere plasmons on the two particles interact and form bonding and antibonding dimer plasmons. Plasmons of different angular momentum on opposite dimer particles also interact to shift dimer plasmons at small separations, shown here for the $l = 1$ derived dimer plasmons. Figure adapted with permission from Reference 28. Copyright 2004 American Chemical Society. (*c*) The plasmon peak is expected to red-shift as two metal nanocrystals in a dimer are brought closer together; here, simulations are done on Au discs. Although larger nanocrystals exhibit greater sensitivity to a change in distance (*top*), a scaling law is predicted for the relative plasmon shift for pairs of Au discs with different diameter size. Figure adapted with permission from Reference 32. Copyright 2007 American Chemical Society.

Figure 5 Metal nanocrystal molecules provide useful tools for microscopy and spectroscopy. (*a*) Dark-field light-scattering spectra from single Au and Ag particles and pairs of particles illustrate plasmon coupling. Scale bar is 3 μm. Figure adapted from Reference 36. (*b*) Plasmon ruler study of DNA cleavage by the EcoRV restriction enzyme. Upon cleavage, the light-scattering spectrum and intensity change abruptly. The single-particle trajectories can be used to observe the sequence of events prior to cutting, including bending of the DNA. Figure adapted from Reference 37.

Figure 6 Gallery of colloidally synthesized semiconductor nanocrystals: transmission electron micrographs of (*a*) CdSe quantum dots, (*b*) CdSe nanorods, (*c*) CdSe tetrapods, (*d*) hollow Co_8O_9 spheres, (*e*) Ag_2S-CdS striped binary nanorods, (*f*) CdSe tetrapods with CdTe dendrimer branches, (*g*) nested Pt@CoO yolk-shell particles, (*h*) Au-tipped CdS nanorods, and (*i*) Bi_2Se_3 nanoflowers. Scale bar is 20 nm.

Figure 7 Nanocrystals are predicted to have shape-dependent optical, electronic, and mechanical properties. Calculated electron (*top row*) and hole (*bottom row*) wave-function charge densities are shown for (*a*) quantum dots, (*b*) nanorods, (*c*) tetrapods, and (*d*) tetrapods compressed uniaxially on the top arm. Panels *a* and *b* adapted with permission from Reference 67. Copyright 2003 American Chemical Society. Panels *c* and *d* adapted with permission from Reference 68. Copyright 2008 American Scientific Publishers.

Figure 8 Semiconductor nanocrystal molecules exhibit altered optical, electronic, and mechanical properties. (*a*) The electron and hole wave-function overlap can be engineered in CdSe/CdS core/shell nanorods by tuning the CdS rod length (*top*) and the electric field (*bottom)*. Figure adapted with permission from Reference 75. Copyright 2005 American Chemical Society. (*b*) Plots of the differential conductance as a function of V and V_g at $T = 5$ K of single nanocrystals. (*i*) A CdSe nanorod, (*ii*) a CdTe tetrapod showing coupled hopping behavior, and (*iii*) a CdTe tetrapod showing delocalized behavior. Insets show scanning electron micrographs of single nanocrystals contacted with electrodes. Figure adapated with permission from Reference 77. Copyright 2005 American Chemical Society. (*c*) Deviatoric stresses induce new radiative transitions in CdSe/CdS core/shell (*i*) dots, (*ii*) rods, and (*iii*) tetrapods. Figure adapted with permission from Reference 69. Copyright 2009 American Chemical Society.

Figure 9 Chemical transformations of nanocrystal molecules. (*a*) Cation exchange reactions enable the reversible transformation of CdSe quantum dots to Ag_2Se quantum dots. Figure taken from Reference 79. Reprinted with permission from AAAS. (*b*) Partial cation exchange enables the formation of CdS-Cu_2S binary nanorod structures; the further addition of copper ions results in full cation exchange of the nanorod. Figure adapted with permission from Reference 81. Copyright 2009 American Chemical Society.

Figure 10 Single colloidal Pt nanocrystal growth trajectories observed via transmission electron microscopy in situ. (*a*) Video images showing simple growth by means of monomer addition (*left column*) or growth by means of coalescence (*right column*). (*b*) Enlarged (1.5 times) color images of panel *a*. Scale bar is 5 nm. Figure taken from Reference 83. Reprinted with permission from AAAS.

Figure 1.

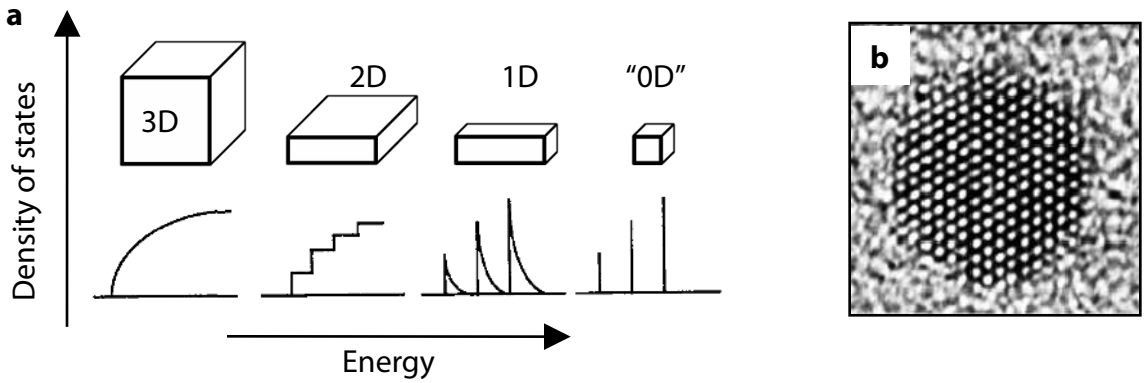

Figure 2.

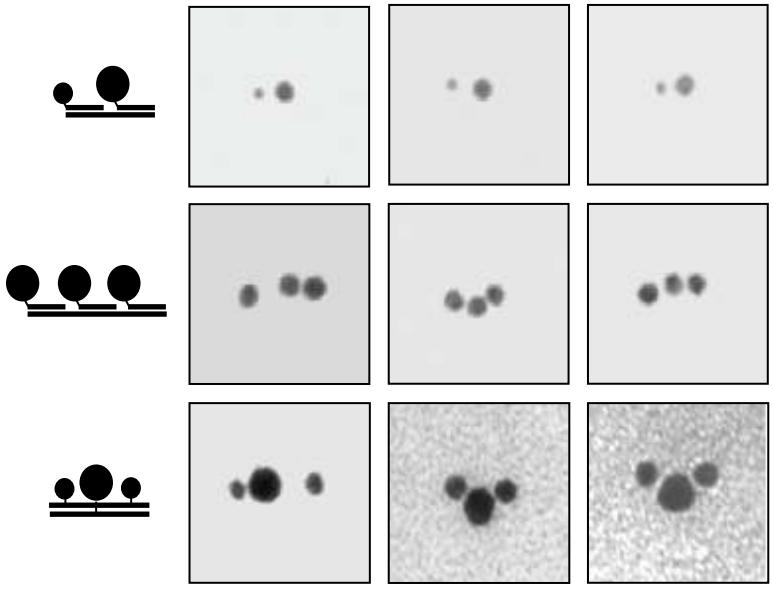

Figure 3.

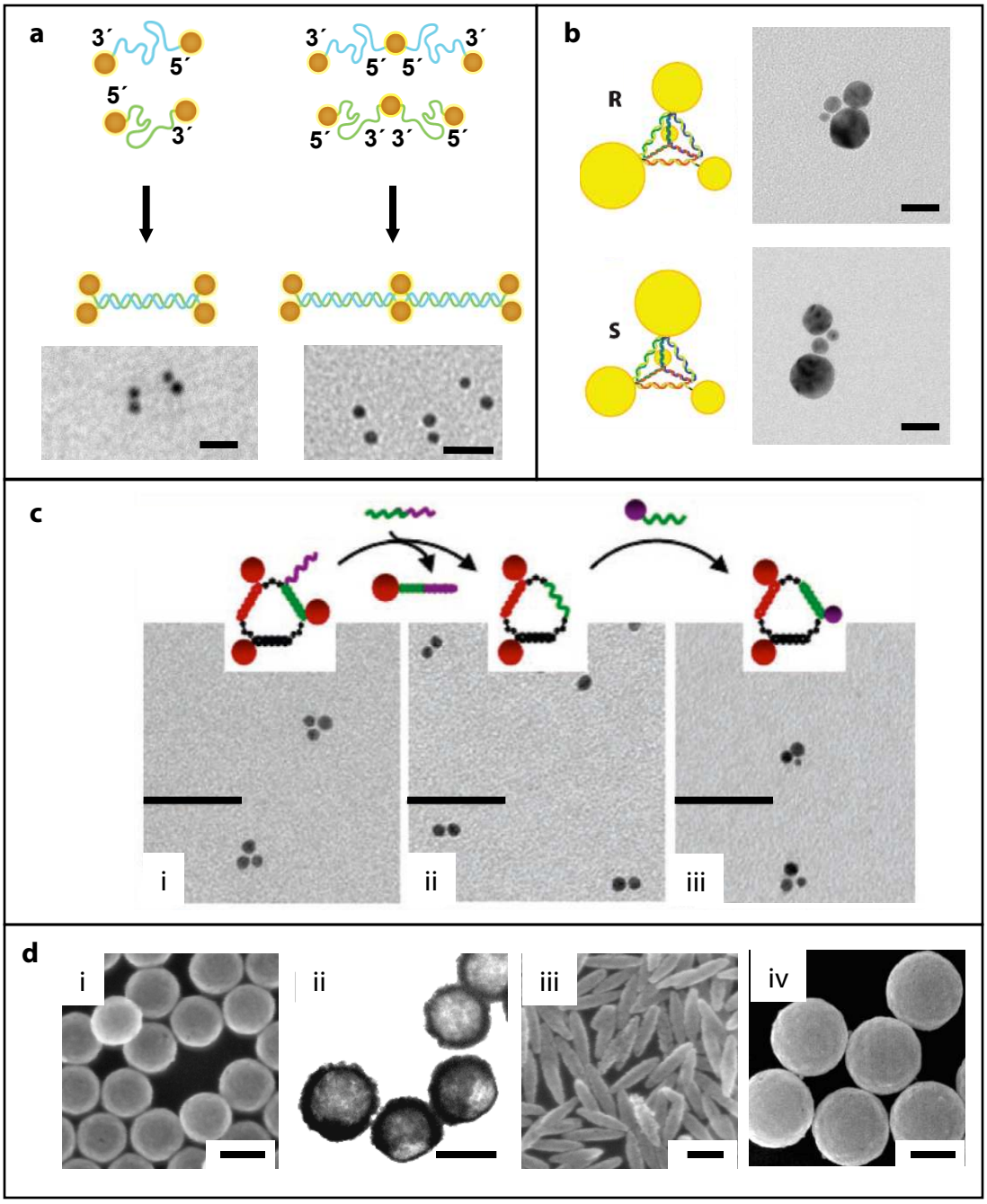

Figure 4.

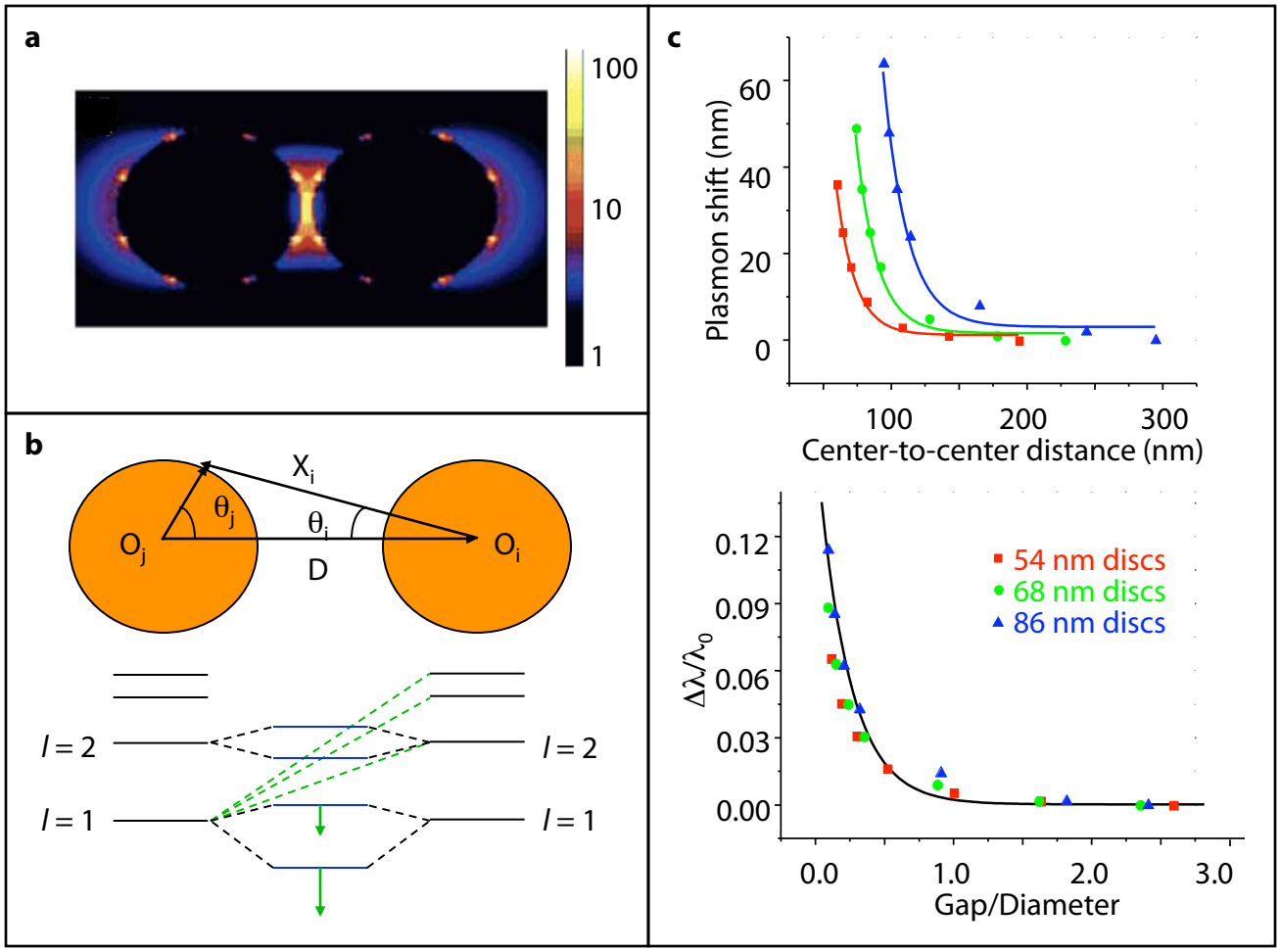
a
100
10
1
b
X_i
θ_j
θ_i
O_j
O_i
D
l = 2
l = 1
l = 2
l = 1
c
Plasmon shift (nm)
60
40
20
0
100
200
300
Center-to-center distance (nm)
Δλ/λ_0
0.12
0.09
0.06
0.03
0.00
54 nm discs
68 nm discs
86 nm discs
0.0
1.0
2.0
3.0
Gap/Diameter

Figure 5.

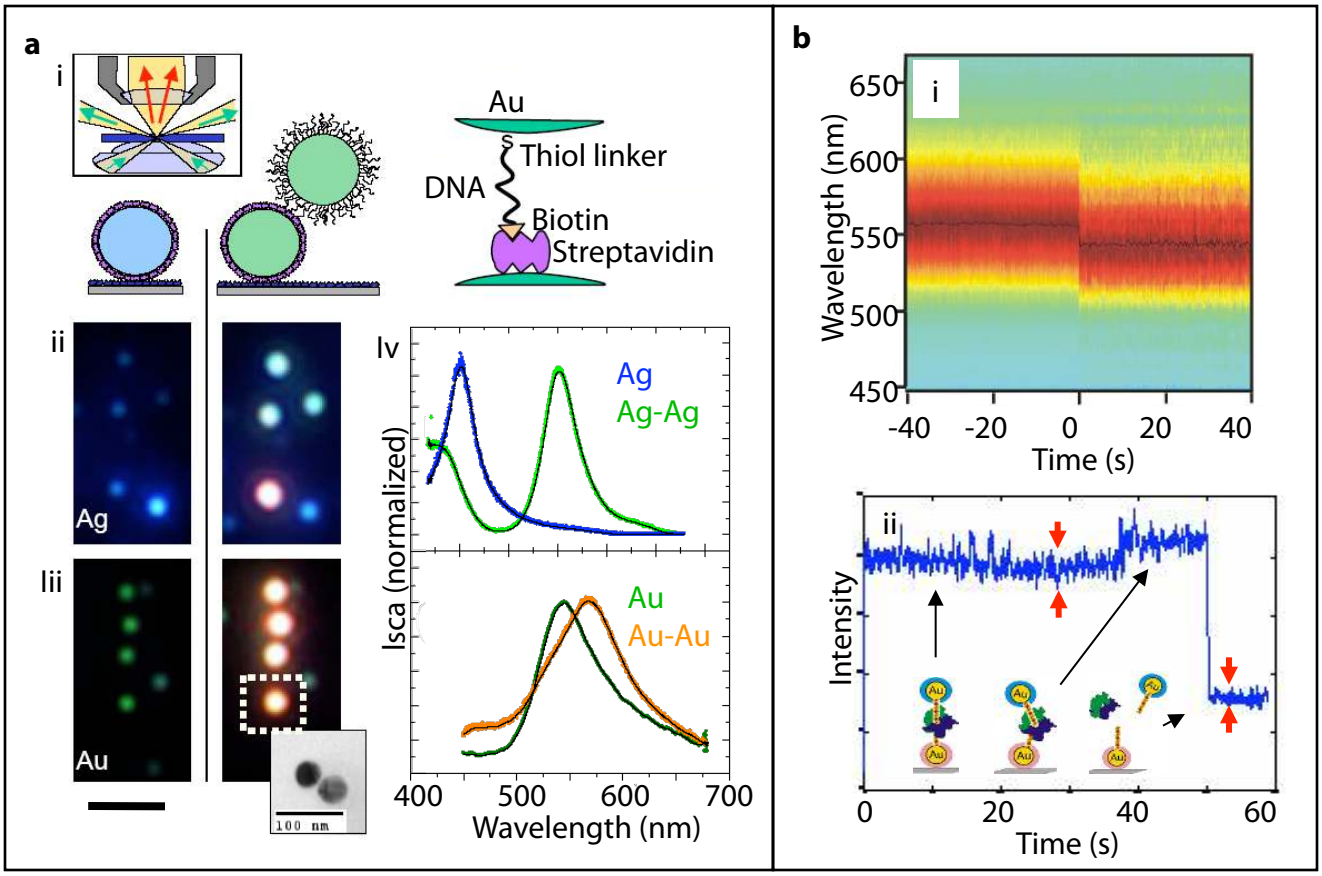
a
i
Au
Thiol linker
DNA
Biotin
Streptavidin
ii
Ag
iii
Au
100 nm
iv
Ag
Ag-Ag
Au
Au-Au
Isca (normalized)
400
500
600
700
Wavelength (nm)
b
i
650
600
550
500
450
Wavelength (nm)
-40
-20
0
20
40
Time (s)
ii
Intensity
0
20
40
60
Time (s)

Figure 6.

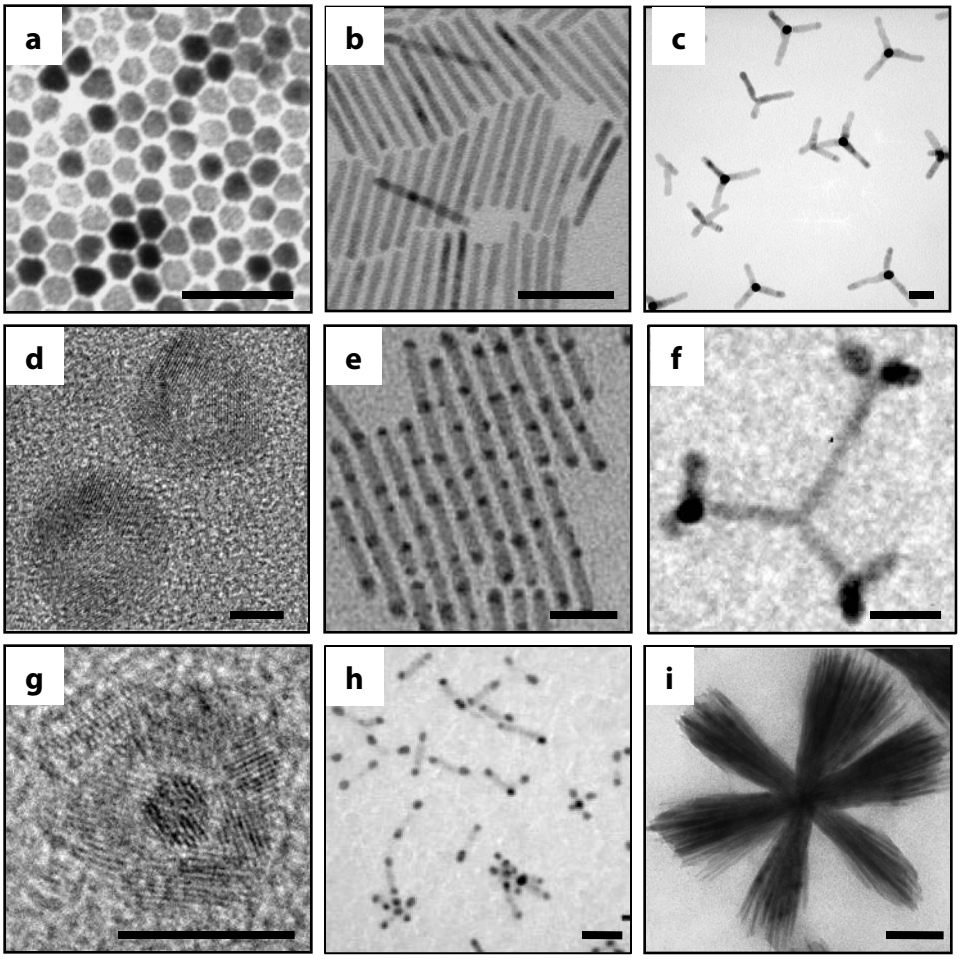

Figure 7.

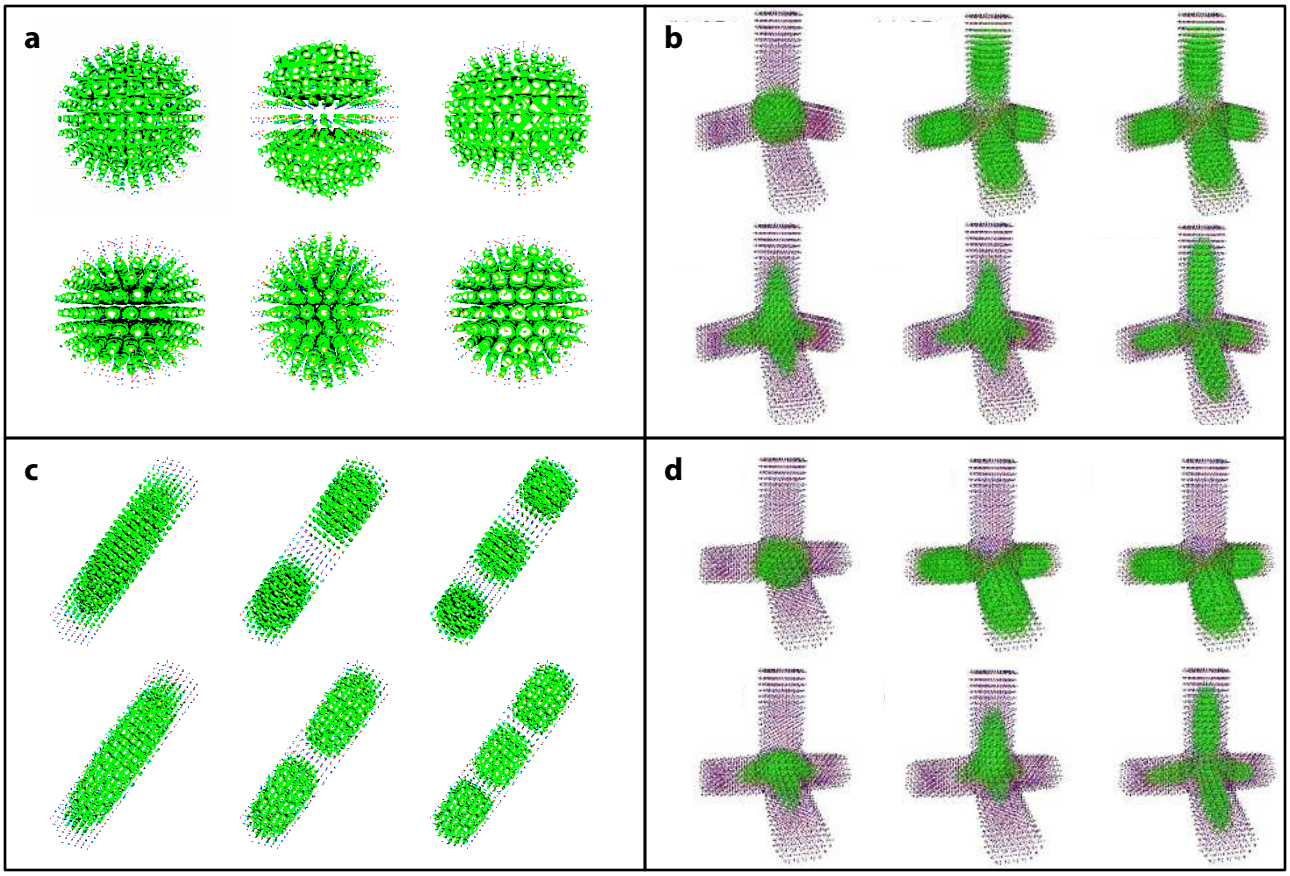

Figure 8.

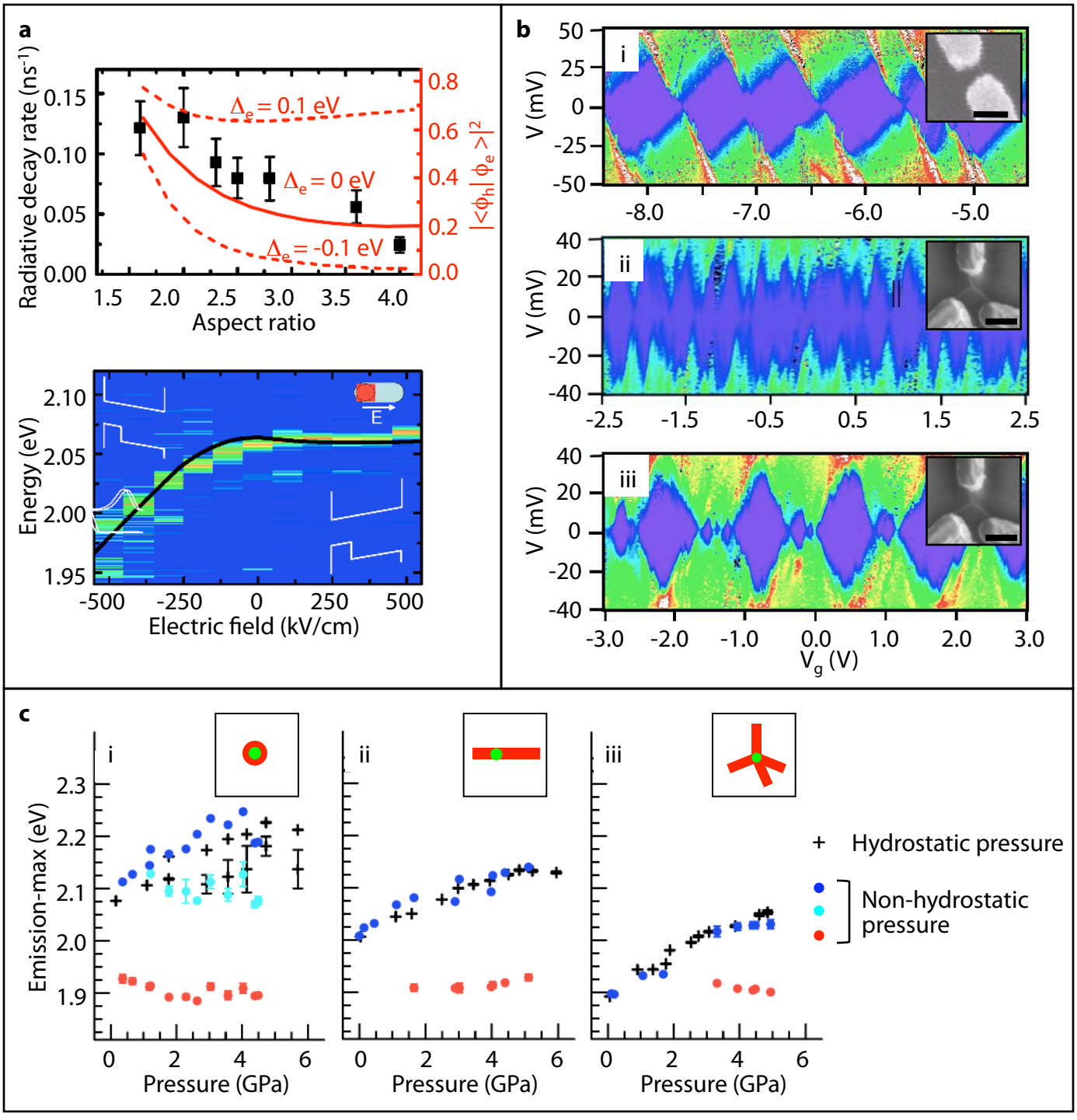
a
Radiative decay rate (ns⁻¹)
0.15
0.10
0.05
0.00
1.5
2.0
2.5
3.0
3.5
4.0
Aspect ratio
Δe = 0.1 eV
Δe = 0 eV
Δe = -0.1 eV
0.8
0.6
0.4
0.2
0.0
|<φh| φe >|²
Energy (eV)
2.10
2.05
2.00
1.95
-500
-250
0
250
500
Electric field (kV/cm)
E
b
i
ii
iii
V (mV)
50
25
0
-25
-50
-8.0
-7.0
-6.0
-5.0
40
20
0
-20
-40
-2.5
-1.5
-0.5
0.5
1.5
2.5
-3.0
-2.0
-1.0
0.0
1.0
2.0
3.0
Vg (V)
c
i
ii
iii
Emission-max (eV)
2.3
2.2
2.1
2.0
1.9
0
2
4
6
Pressure (GPa)
+ Hydrostatic pressure
Non-hydrostatic pressure

Figure 9.

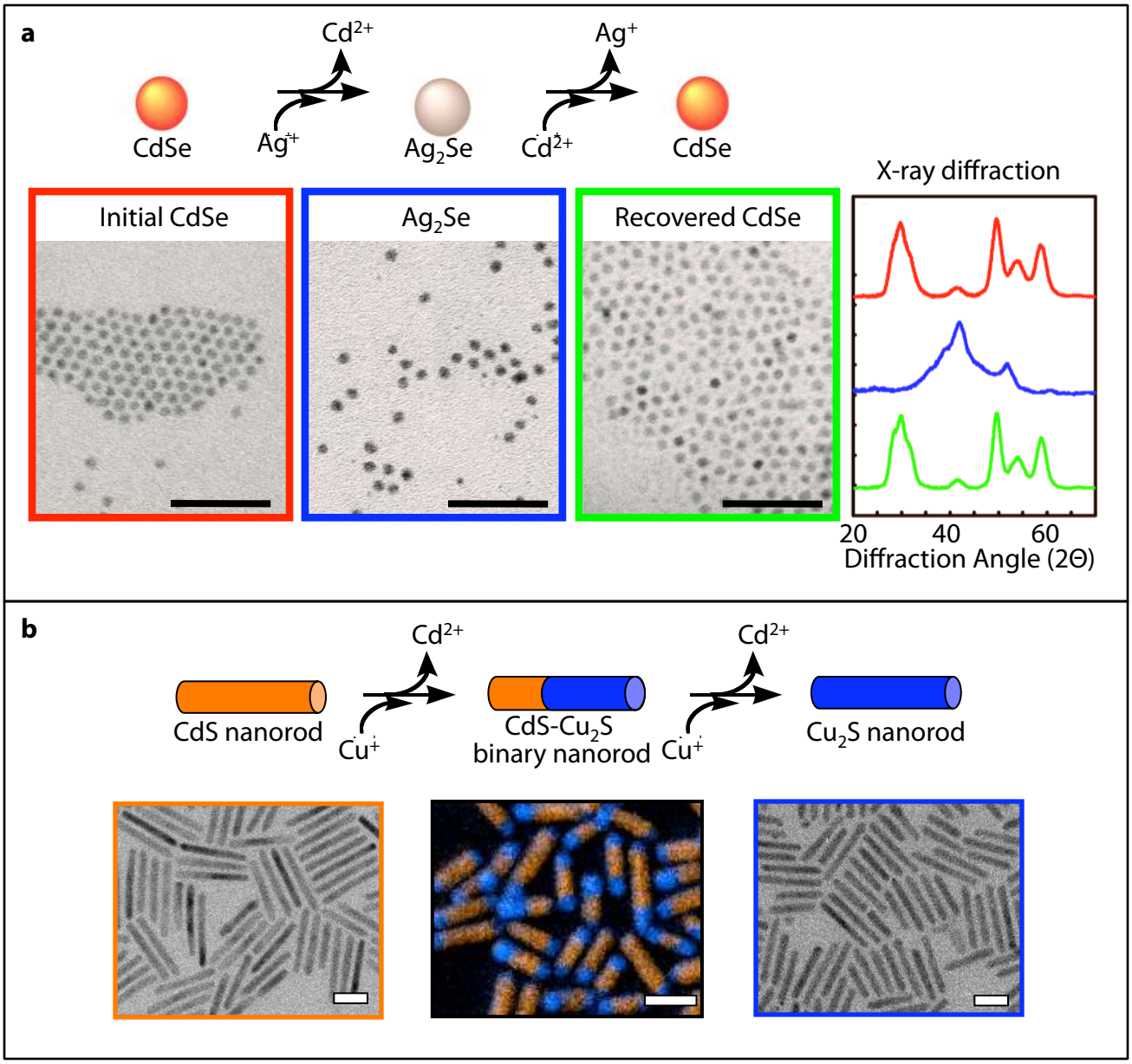
a
Cd2+
Ag+
CdSe
Ag2+
Ag2Se
Cd2+
CdSe
X-ray diffraction
Initial CdSe
Ag2Se
Recovered CdSe
20
40
60
Diffraction Angle (2Θ)
b
Cd2+
Cd2+
CdS nanorod
Cu+
CdS-Cu2S
binary nanorod
Cu+
Cu2S nanorod

Figure 10.